Modular TEMPO Dimerization for Water-in-Catholyte Flow Batteries with Extreme Energy Density, Power, and Stability

Xiu-Liang Lv[a†], Patrick T. Sullivan[b†], Wenjie Li[b*], Hui-Chun Fu[b], Ryan Jacobs[a], Chih-Jung Chen[b], Dane Morgan[a], Song Jin[b], and Dawei Feng[ab*]

[a] Department of Materials Science and Engineering, University of Wisconsin-Madison, Madison, Wisconsin, USA

[b] Department of Chemistry, University of Wisconsin-Madison, Madison, Wisconsin, USA

† These authors contributed equally to this work

* e-mail: wli@chem.wisc.edu; dfeng23@wisc.edu

Abstract: Aqueous organic redox flow batteries (AORFBs) hold great promise for safe, sustainable, and cost-effective grid energy storage. However, developing catholyte redox molecules with desired energy density, power, and stability simultaneously has long been a critical challenge for AORFBs. Here, we report a novel class of ionic liquid mimicking TEMPO dimers (i-TEMPODs) that can be produced by our newly developed building block assembly synthetic platform. By systematically investigating 21 derivatives, we reveal i-TEMPODs have optimized size and charge that is compatible with highly conductive membrane and can form a "water-in-catholyte" (WiC) state. The tight coordination dynamics with water molecules deliver extreme solubility with promoted electrochemical stability at highly positive potentials. Leveraging these advances, we identify a champion molecule and demonstrate record overall AORFB performance in energy density (47.3 Wh L^{-1}), power density (0.325 W cm^{-2}), and stability (no apparent capacity decay after 96 days) with low-cost and scalable chemistry.

Redox flow batteries (RFBs) are a promising grid energy storage technology offering scalable and adaptable system design through the decoupling of power and capacity components. Vanadium redox flow batteries (VRFBs) have found commercial application due to their high capacity (1.6-3.0 M Vanadium ions electron concentration), energy density (25-35 $Wh \cdot L^{-1}$), and capacity rebalancing ability.[1] However, the resource constraints and volatile pricing of vanadium limit the widespread application of VRFBs[2] and have stimulated the development of aqueous organic redox flow batteries (AORFBs),[3–10] which employ water-soluble organic redox active molecules as the anolyte and catholyte. Despite significant recent progress, AORFBs with energy density and stabilities comparable to commercialized VRFBs have not yet been developed.[11–13]

Most existing redox active organic molecules designed for RFBs share a common challenge of concurrently delivering high volumetric capacity and cycling stability: molecules of smaller size tend to possess enhanced solubility and lower viscosity at high concentration, promoting larger volumetric densities, but they permeate through ion-exchange membranes at a greater rate, accelerating capacity decay and lowering columbic efficiency. Increasing the molecular size with extended carbon chains and additional charge (i.e., quaternary ammonium, sulfonate, phosphonate, and carboxylate) has partially deterred material crossover,[6] but this strategy sacrifices volumetric capacity when comparing small and large water-miscible compounds (Fig. 1). This is because the added redox inactive mass increases the molecular size and intermolecular forces (both London dispersion and electrostatic) that inhibit space-efficient packing of the electrolyte molecules in solution, limiting solubility and increasing viscosity. Thus, new scientific approaches for designing redox molecules are needed to circumvent this seemingly inherent conflict between volumetric capacity and stable cycling in AORFBs.

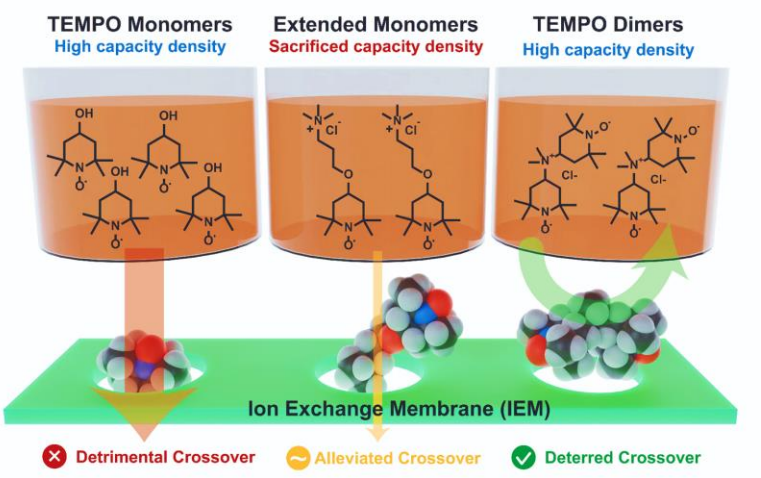

Fig. 1 | The TEMPO dimer molecular design circumvents the tradeoff between capacity and crossover of redox active molecules in conventional extended monomer strategies.

While a lot of research for AORFBs has been devoted to the development of anolyte (negolyte) redox molecules, such as quinones,[14,15,24,16–23] viologens,[25–34] and phenazines,[35–40] stable catholyte (posolyte) species with high capacity are scarce yet equally important in full cells.[11] Among all the studied catholyte molecules, (2,2,6,6-Tetramethylpiperidin-1-yl)oxyl (TEMPO) derivatives represent one of the most promising redox cores due to its stable redox behavior, high redox potential (> 0.8 V vs. SHE), solubility as high as 2 M demonstrated cycling for TEMPTMA (N^{Me}-TEMPO), [41] and low cost. However, TEMPO molecules reported for RFBs suffer from severe crossover due to their smaller size than the ion-conductive channels in ion-exchange membranes (IEMs) (Fig. 1), especially in low resistance membranes.[32,41–48] Recent efforts have significantly improved the cycling stability performance of TEMPO derivatives upon the earliest AORFB demonstration of OH-TEMPO[32] through appending charged groups and extended tails to the 4-position, but there are still significant extrapolated capacity decay rates and/or dramatically sacrificed volumetric capacity that prevents commercial application: TMAP-TEMPO demonstrated a decay rate of 227.8% per year at 1.5 M,[47] N_2-TEMPO has an estimated

decay rate of over 200% per year at 1 M,[46] and Pyr-TEMPO showcased a decay rate of 1,267% per year at 0.5 M.[45] Hence, building on the knowledge gleaned in previous works, new design strategies must be explored to prevent crossover of TEMPO derivatives while retaining high volumetric capacity.

Herein, we present a novel class of molecular engineered ionic-liquid mimicking TEMPO dimers (i-TEMPODs) to address the challenging performance tradeoffs in AORFBs. i-TEMPODs are comprehensively established with a specifically designed building block assembly synthesis strategy. Leveraging this high-throughput platform, we systematically synthesize and characterize 21 i-TEMPOD molecules and reveal that the water miscibility of i-TEMPODs can enable a water-in-catholyte (WiC) state through strong water coordination environment and to achieve record catholyte volumetric capacity (101 Ah L^{-1} catholyte demonstrated) and full cell energy density (47.3 Wh·L^{-1}). Through membrane compatibility and a strong water coordination environment, the champion molecule, N+TEMPOD, demonstrated stable cycling performance without observable capacity decay at 4 M electron concentration for over 96 days. A maximum power density of 0.325 W cm^{-1} was also demonstrated with stable cycling, which is unprecedented for pH neutral AORFBs and on par with alkaline AORFBs. This work highlights the significantly improved RFB performance of i-TEMPODs over the state-of-the-art AORFB catholytes.

There are several key factors for our successful TEMPO dimer design. Firstly, many redox active organic cores, including viologens, anthraquinones and phenazine, rely on large aromatic structures to stabilize their redox active states. This renders their dimers unsuitable as the inter- and intra- molecular π-π stacking interactions will be too strong in either the reduced or oxidized states to maintain high solubility and low viscosity during cycling in aqueous electrolyte.[49] In contrast, TEMPO core consists of only sp^3 carbons which offers weak intermolecular interaction

dominated by London dispersion forces. Dimerized TEMPOs retain low intermolecular interaction and thus remain highly water miscible when attached to an ionic group with strong hydrophilicity. Secondly, when an imidazolium, pyridinium, or quaternary ammonium-based bridge linker is introduced to connect two TEMPOs (Fig. 2a), water miscibility is obtained with ionic-liquid mimicking i-TEMPOD structures.[50,51] Thirdly, the size of the TEMPO dimers prevents crossover through IEMs, even those with larger pores and ionic conductivities that permit high RFB power density. Finally, the minimal redox inactive structural component in these TEMPO dimers promotes optimized spatial occupation of TEMPO cores per unit volume to form a "water-in-catholyte" (WiC) composition, similar to the concept of "water-in-salt"[52–59] to achieve extremely high volumetric capacity and stability at high voltage.

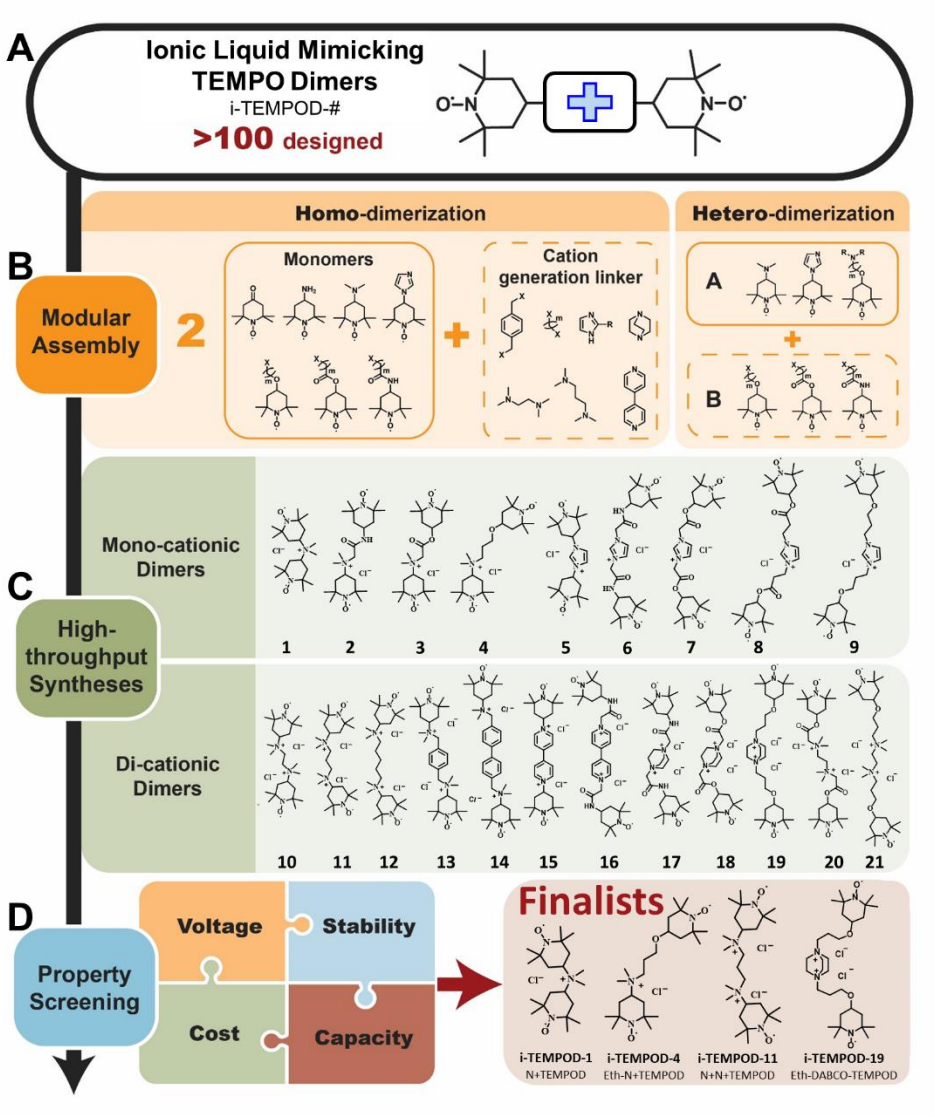

Fig. 2 | The modular building-block assembly synthetic strategy of ionic liquid mimicking TEMPO dimers (i-TEMPODs). a, General design of i-TEMPOD structure consisting of TEMPO cores linked by a soft cationic bridge, from which over 100 derivatives were devised. **b**, The reactive building blocks, including TEMPO cores of varying 4-position functionality and linkers as cationic bridges. **c**, The 21 synthesized i-TEMPODs that were characterized through high-throughput property screening. **d**, The 4 champion i-TEMPODs selected for RFB cycling study based on systematic multi-objective performance optimization.

Bearing in mind the i-TEMPOD design, we comprehensively establish this new class of TEMPO derivatives by structurally designing 101 such ionic TEMPO dimers and 17 oligomers (trimers and tetramers) (Fig. S1-3). To promote high-throughput production of i-TEMPODs, we developed a building block assembly synthetic strategy (Fig. 2b). Firstly, we synthesized both reactive TEMPO units that store redox active electrons and linkers that connect TEMPO cores with a cationic bridge (Fig. S4-8). These building blocks were rationally designed to be universally applicable in simple, efficient substitution and elimination reaction steps. Next, these units were assembled in either homo-dimerization pathway by linking two identical TEMPO monomers with a bridging unit or hetero-dimerization pathway by linking TEMPO monomers with different type of functionalization group at the 4-position of TEMPO unit. This step allowed building of various positively charged TEMPO dimers structures with different chemical, electrochemical, and physical properties. Considering synthetic simplicity, 21 i-TEMPODs (Fig. 2c) were produced among the over 100 designed structures, structurally confirmed (Fig. S9-29), and electrochemically characterized (Fig. S37-57). Finally, with systematic multi-objective performance optimization of identifying metrics – feasible capacity (solubility and viscosity), electrochemical stability (redox kinetics and potential) and cost (precursor availability and synthetic ease) –representative TEMPO dimers were selected for further in-depth evaluation (Fig. 2d).

To delineate structure-property relationships for molecular engineering of TEMPO dimers, we evaluated the formal potential (E^o) of each i-TEMPOD using cyclic voltammetry (CV) (Figs. S37-57). All 21 exhibited highly positive E^o values ranging from +0.804 V to +0.981 V vs. SHE that are near the thermodynamic oxygen evolution reaction (OER) potential limit (0.82 V vs. SHE) of neutral pH aqueous electrolyte (Fig. 3a and Table S2). Additionally, a clear relationship between

E^o and the electronic properties of the 4-position functionalization for TEMPO derivatives is revealed. As the electron withdrawing strength of the functionalization increased, more energy is required to remove an electron from the TEMPO core, leading to a higher E^o. Accordingly, the E^o of the TEMPO dimer and thus the output voltage of the RFB can be tuned based on the 4-position functionalization as follows: ether < amide ≈ ester < imidazolium/pyridinium < quaternary ammonium. Meanwhile, linker identity away from the 4-position of TEMPO core had minimal effect on E^o. Although highly positive E^o is desired for increasing the output voltage and ultimately improved power and energy density performance of the RFB, other dependent factors, such as synthetic cost, chemical stability, and cathodic OER competition must also be considered when designing catholyte redox molecules to optimize overall RFB performance. Based on these factors, two mono-cation dimers (N+TEMPOD and Eth-N+TEMPOD) and two di-cation dimers (N+N+TEMPOD and Eth-DABCO-TEMPOD) were selected for further characterization. These four i-TEMPOD finalists each demonstrated facile diffusion and electron transfer kinetics in CV (Fig. S59-65). and Electrochemical Impedance Spectroscopy (EIS) study (Fig. S67 and Table S3). We found a negative correlation between electron transfer rate constant (k^0) and molecular size for these dimers but no trend with 4-postion functionalization (Table S4).

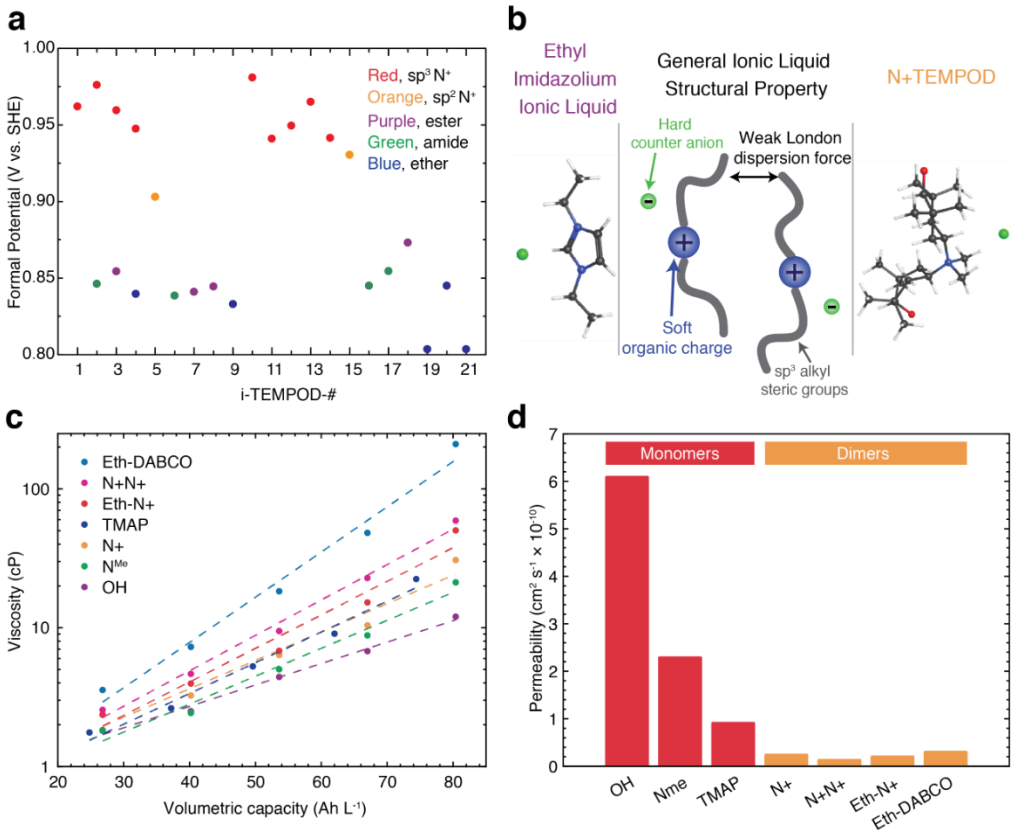

Fig. 3 | Key electrochemical and physiochemical metrics of TEMPO dimers. a, The formal potential of all 21 synthesized i-TEMPOD-# demonstrating tunability to reach the OER potential limit by modifying the 4-position functionality. **b**, Ionic liquid mimicking design of TEMPO dimers to enable WiC state. **c**, Logarithmic viscosity-volumetric capacity relationship for selected TEMPOs monomers and dimers with empirical exponential fits. **d**, Permeability of different TEMPOs through high-power DSVN anion-exchange membrane tested in H-cells. The TEMPO dimers showed orders of magnitude decreased permeability versus TEMPO monomers.

i-TEMPODs have extremely high water solubility and can form a water-in-catholyte (WiC) state when saturated. The i-TEMPODs exactly mimic the features of ionic liquid molecules (Fig. 3b).[50,51] Such a structure ensures water miscibility as the "soft" cationic motif with a "hard" anion pair offers strong affinity to water molecules and the sp^3 carbon chains prevent self-intimate

packing of charged parts. For non-phenyl ring containing TEMPO dimers, their solubility in pure water ranged from 1.7 M to 2.5 M (Table S4), corresponding in 3.4 M to 5 M redox active electron concentrations. This heightened theoretical maximum capacity of dimers ultimately results from increasing the size of the TEMPO core at the 4-position with redox active mass (i.e., other TEMPO cores) and without significantly increasing electron averaged mass (M/n). This contrasts extended TEMPO monomer strategies that inflate the mass with redox inert functionalization.[45–47] Saturated dimer solutions have an average density of 1.25 $g \cdot mL^{-1}$, resulting in an estimated range of 1 to 20 water molecules per TEMPO dimer (Table S5). Moreover, under WiC dynamics, the stable voltage window of water was extended because there are the limited water molecules will be within the inner solvation sphere with strong intramolecular force between the redox molecules. This could significantly increase kinetic barriers of OER at the electrode surface,[52–59] which is especially instrumental for catholytes with highly positive formal potential, such as TEMPOs. These advances make the WiC state a critical feature of i-TEMPODs to the concurrently achieve high capacity and high cycling stability.

When determining the maximum cycling concentration with the water-miscible i-TEMPODs, the active molecule solubility (hydrophilicity) no longer limits volumetric capacity. The interaction between the dissolved i-TEMPODs and the water molecules is very thermodynamically favorable, and each i-TEMPOD is able to dissolve with a minimal amount of coordinated water. The cycling concentration is instead limited by the electrolyte viscosity and its relation to pumping efficiency. Therefore, we experimentally measured the viscosity of representative TEMPO monomer and dimer solutions at various volumetric capacities in their reduced (uncharged) states (Fig. 3c). When comparing TEMPO dimers, viscosity increases with molecular weight and the number of positive charges because these two factors both increase intramolecular interactions.

These data provide valuable insight into designing water-miscible TEMPO dimers with optimized energy density. The smallest dimer, N+TEMPOD (**1**), has nearly equal viscosity at a given volumetric capacity to the state-of-the-art extended monomer, TMAP-TEMPO. It is also worth noting that for all TEMPO species, viscosity is expected to increase upon oxidation (charging) because of the additional oxoammonium positive charge. This hypothesis was confirmed through ab initio Molecular Dynamics (AIMD) simulations of N+TEMPOD in water by calculating the diffusivity of the redox molecule in both reduced and oxidized forms (Fig. S68). The oxidized form of N+TEMPO showed 35% lower diffusivity in water compared to the reduced form, indicating higher viscosity of the oxidized form (Fig. S69). The AIMD simulation results unveil coordination environments between water and redox and their changes during cycling influence RFB flow properties.

Although for maximized volumetric capacity it would be ideal to select the least viscous TEMPO catholyte, such as N^{Me}-TEMPO or OH-TEMPO (Fig. 3c), such low viscosity usually entails lower molecular weight and charge for those previously demonstrated TEMPOs, which in turn sacrifices IEM size exclusion and charge repulsion. This was demonstrated by measuring the permeability of the TEMPO species through low ionic-conductivity anion-exchanged membrane (AMVN, Table S8). As expected, the permeability of for TEMPO monomers drastically increases as the size decreases. In contrast, each i-TEMPOD finalist, including even the smallest N+TEMPOD, displays compatibility and no detectable crossover with AMVN membrane. Crossover of the TEMPO species is detrimental to RFB lifetime as it lowers the catholyte capacity through material loss and the anolyte capacity through chemical/electrochemical side reactions (Fig. S70). Previously reported monomeric TEMPOs, OH-TEMPO, N^{Me}-TEMPO, and TMAP-TEMPO demonstrated drastic decay rates of 3.88%/day, 0.30%/day, and 0.89%/day (Fig. S71a),

respectively, when cycled with AMVN membrane in a catholyte-limiting configuration with our previously reported ultra-stable and low-cost viologen anolyte, Dex-Vi.[60] In contrast, each i-TEMPOD demonstrated no observable decay (Fig. 4a-d) when following the same RFB cycling protocol. Even at a high concentration of 2 M N+TEMPOD (4 M electron concentration), no capacity decay was shown after 96 days of cycling (Fig. 4e).

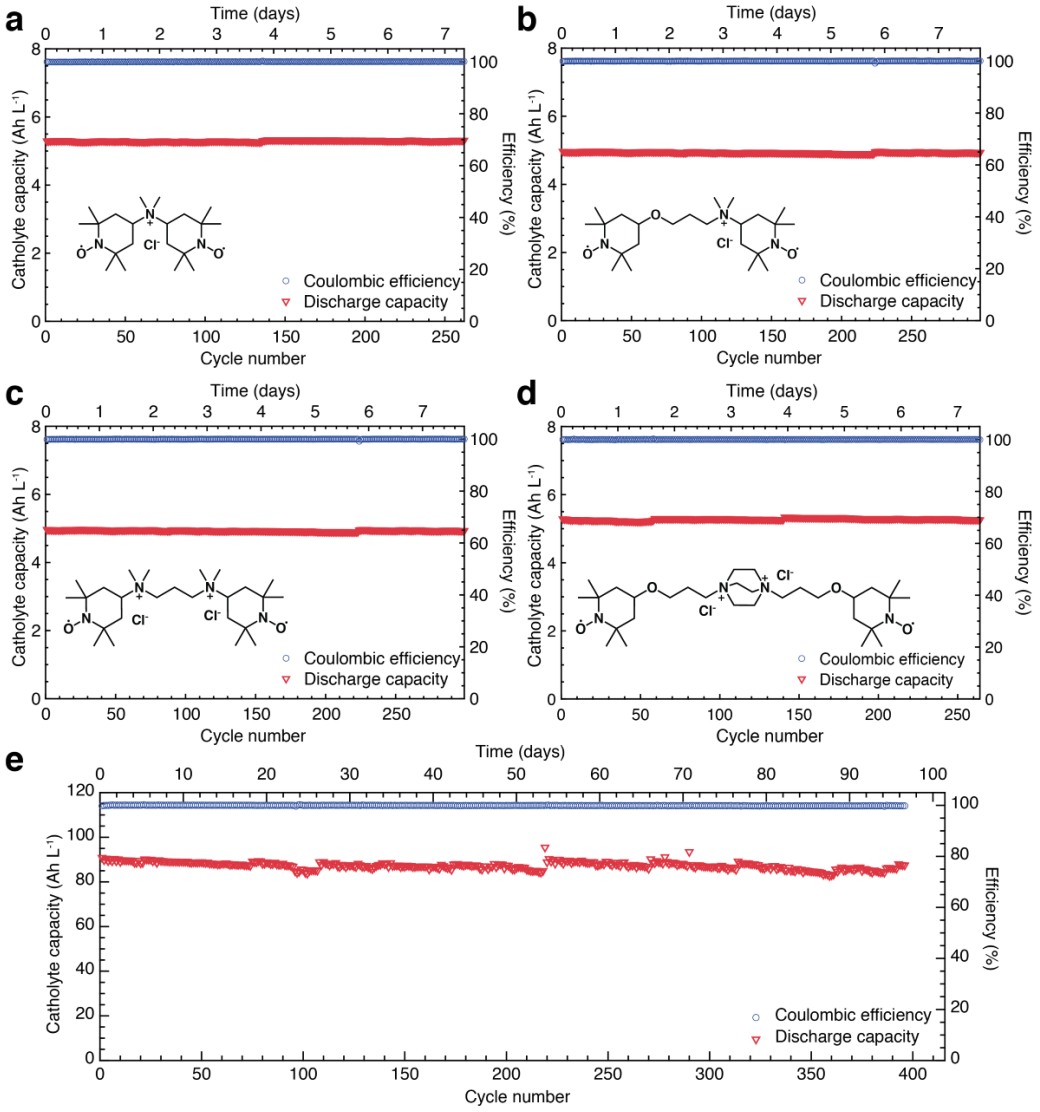

Fig. 4 | RFB cycling performance demonstrated with low ionic-conductivity AMVN membrane of four representative TEMPO dimers. a-d, Low concentration RFB cycling profile

of N+TEMPOD (**a**), Eth-N+TEMPOD (**b**), N+N+TEMPOD (**c**), and Eth-DABCO-TEMPOD (**d**) with 0.1 M TEMPO dimer and 1.5 M NaCl as catholyte (capacity-limiting side) and 0.2 M Dex-Vi and 1.5 M NaCl as anolyte. **e**, High concentration, long term RFB cycling profile with 2.0 M N+TEMPOD as catholyte (capacity-limiting side) and 1.0 M Dex-Vi as anolyte at room temperature. Intermittent capacity increases correspond to manual shaking of the electrolyte reservoir in which portions of the viscous solution were recovered into the flow stream.

For AORFBs with kinetically facile redox species, such as TEMPO, the device resistance and power capability are mainly limited by membrane resistance. For example, for high concentration N+TEMPOD flow battery with AMVN membrane at 50% state-of-charge (SOC), the membrane resistance [estimated from high-frequency area-specific resistance (r_{hf}), 2.72 Ω cm^2] was 94.8% of the total cell resistance [estimated from DC polarization area-specific resistance (r_{DC}), 2.87 Ω cm^2] (Fig. 5b). Reported RFB cycling demonstrations of TEMPO monomers have usually sacrificed power for stability with low-power, highly selective AMV/AMVN anion-exchange membrane.[45–47] To showcase this important but often overlooked metric for evaluating TEMPO performance, we conducted systematic comparison of the RFB power and cycling performances with AMVN and DSVN membranes for the TEMPO monomers and dimers. The r_{DC} of the DSVN flow cell (1.26 Ω cm^2) was 43.9% of that of the AMVN flow cell (2.87 Ω cm^2) at 50% SOC (Fig. 5a). Enabled by the high conductivity of DSVN membrane, high concentration N+TEMPOD RFB with a formal cell potential of 1.19 V (OCV at 50% SOC, Fig. 5a) displayed a peak power density of 0.325 W cm^{-2} (Fig. 5b). Further cycling experiments of the RFB at different current densities revealed a capacity utilization rate of 97.4% and a roundtrip energy efficiency (EE) of 86.1% at 60 mA·cm^2 (Fig. 5c, d). In contrast, the RFB with AMVN membrane exhibited a sacrificed EE of 75.1% under identical conditions (Fig. S72). The power capability demonstrated here is

unprecedented for pH neutral AORFBs, which typically can only deliver peak power densities of below 100 $mA \cdot cm^{-2}$ and EE of 60-70% at similar current density[25,46,47,61] and is on par with alkaline AORFBs which have boasted higher power performance than pH neutral RFBs to date.[14,19,36,62] Such high-power performance had previously been unrealized for pH neutral AORFBs because decreased membrane resistance was often accompanied by severe crossover of small organic redox species and thus poor cycling stability. Each TEMPO monomer showed high DSVN permeability and poor cycling stability with capacity decay rates of 4.35%/day, 0.66%/day, and 1.53%/day for OH-TEMPO, N^{Me}-TEMPO, and TMAP-TEMPO, respectively (Fig. S71b). In contrast, the smallest i-TEMPOD, N+TEMPOD, demonstrated deterred permeability and remarkable capacity retention in high-concentration RFB cycling test with DSVN membrane (Fig. 5e). This confirms high cycling stability, high power, and high volumetric capacity can be simultaneously accomplished with i-TEMPODs.

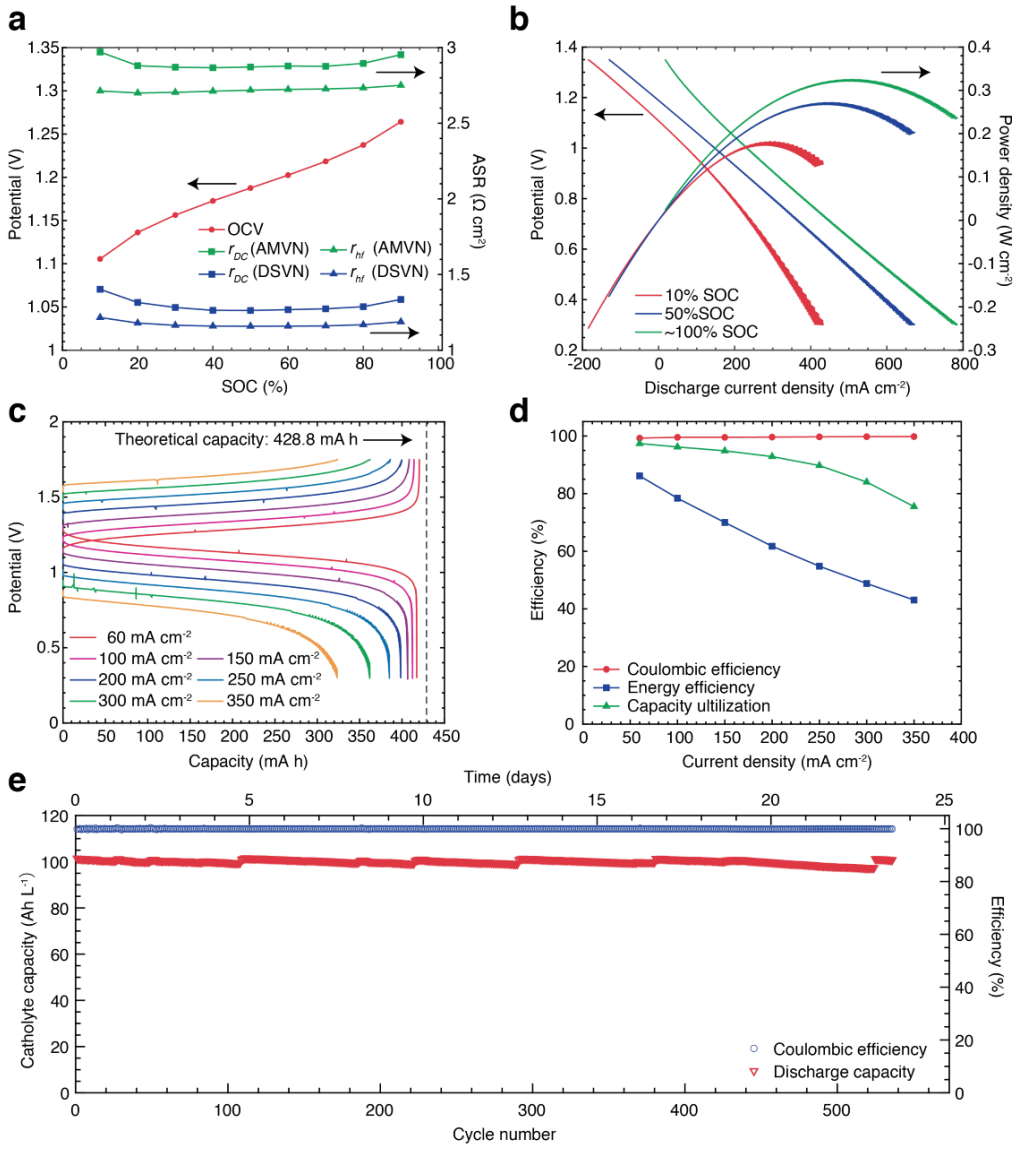

Fig. 5 | RFB power and cycling performance with high ionic-conductivity DSVN membrane. **a**, Open circuit voltage (OCV) and area-specific resistance (ASR) measured at different SOCs. The ASR of another RFB cell with AMVN membrane and the same electrolyte composition was also presented as a comparison. **b**, DC polarization curves measured at 10%, 50% and near 100% SOCs, showing cell potential and power density versus current density. The cell reached a maximum discharging power density of 0.325 W cm^{-2} at near 100% SOC. **c**, Cell potential profile with respect to cell capacity at different cycling rate. **d**, Coulombic efficiency, round-trip energy

efficiency and capacity utilization at different cycling rate. **e**, High concentration, long term RFB cycling profile showing stable cycling performance over 23 days. 2.0 M N+TEMPOD and 1.0 M Dex-Vi were used as catholyte (capacity-limiting side) and anolyte, respectively, for all the measurements presented herein. Intermittent capacity increases correspond to manual shaking of the electrolyte reservoir in which portions of the viscous solution were recovered into the flow stream.

The overall catholyte performance demonstrated herein – voltage, volumetric capacity, power, and stability – is unprecedented in AORFB systems (Fig. 6a, Table S9). Other than TEMPO redox species, catholytes for pH neutral AORFBs have been largely limited to iron organometallic complexes, including iron cyanide,[63] iron bipyridine,[64] and ferrocene derivatives.[65–68] These iron-based catholytes typically suffer from low formal potentials far below the pH neutral water OER potential limit due to the intrinsic high HOMO energy level of the iron redox active electron. This HOMO energy level can be lowered through ligand electronic properties to result in more positive formal potentials, such as with the symmetry breaking iron bipyridine complex,[64] but this results in a drastic tradeoff in cycling stability.[12] In contrast, all TEMPO derivatives demonstrate highly positive formal potentials and facile kinetics due to the redox properties of the nitroxide radical. Crossover of TEMPO has been classically mitigated by extension of the TEMPO monomer 4-position, which sacrifices volumetric capacity.[45–47] However, with the i-TEMPOD design and resulting WiC state, high volumetric capacity, stability, voltage, and power can be concurrently achieved. To fully demonstrate the advantage of i-TEMPODs, we paired N+TEMPOD with a new viologen anolyte (Dex-EtOH-Vi, Fig S58) and demonstrated a full cell energy density of 47.3 Wh L^{-1} (Fig. S73), which far surpassed that of all the previously demonstrated AORFBs and was on par with state-of-the-art commercial VRFBs (Fig. 6b).

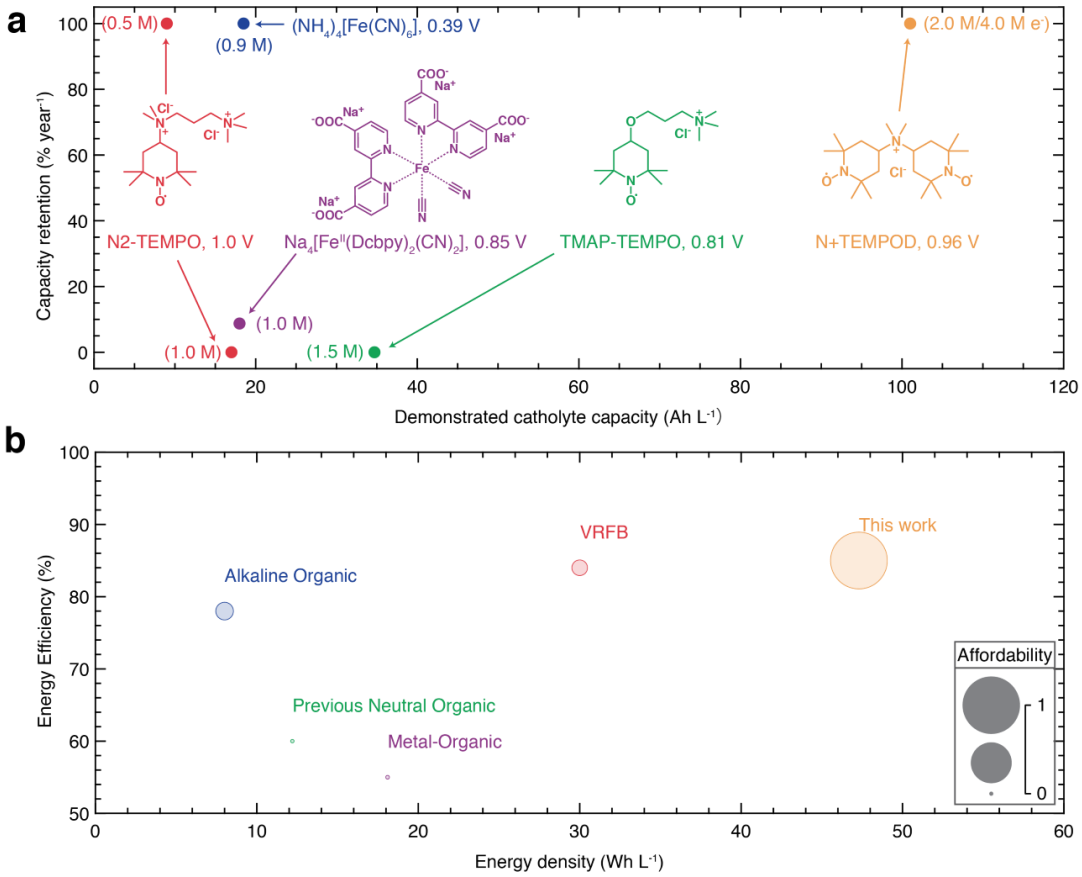

Fig. 6 | Key performance metrics of the i-TEMPOD RFB in comparison with other state-of-the-art grid energy storage technologies. a, Comparison of the demonstrated catholyte capacity and yearly capacity retention of N+TEMPOD with other representative pH neutral AORFB catholytes. **b**, Full cell energy density, energy efficiency (at 60 mA cm^{-2}) and affordability (displayed as the size of the circles) of different types of aqueous RFBs. Affordability was estimated based on the inversion of lab-scale chemical cost (per Wh) normalized by the cost of N+TEMPOD/Dex-EtOH-Vi RFB presented in this work.

In addition to record catholyte performance, the i-TEMPODs utilize readily available starting materials and efficient synthetic methods. For example, N+TEMPOD was synthesized at $4.76/Ah ($0.16/g) on the lab-scale considering starting material cost and yield (Table S9). The lower lab-scale cost of i-TEMPODs compared to other redox species asserts their potential pricing

advantage in addition to the extremely high RFB performance for grid-scale energy storage application (Fig. 6b, Table S14). This is in addition to offering improved fire safety, enhanced material sustainability and supply chain security, and heightened system scalability and adaptability. Through the fundamental molecular design, synthesis strategy optimization, systematic screening, and in-depth physical, chemical and electrochemical study of i-TEMPODs in this work, we paved the way for an economical and reliable clean energy transition with long-duration AORFBs.

Methods

Synthesis of i-TEMPODs:

The i-TEMPOD catholyte molecules were, in general, synthesized by linking together two reactive TEMPO building block reagents. For example with N+TEMPOD, f4-Oxo-TEMPO (20 g, 117.7 mmol) 4-Amino-TEMPO (20 g, 116.8 mmol) were dissolved in anhydrous MeOH (100 mL) under N_2 protection and sealed in a thick-walled pressure bottle. After the mixture was stirred for 20 min at room temperature, acetic acid (2 mL) was added, and the resulting solution was stirred for 20 min at room temperature. Next, sodium borohydride (366 mg, 5.84 mmol) was added at once and the mixture was then refluxed for 50 h. The reaction mixture was then diluted with DCM (20 mL), and saturated aqueous $NaHCO_3$ solution (100 mL) with water (100 mL) was added. The separated aqueous layer was extracted with DCM (200 mL). The combined organic phases were dried over anhydrous Na_2SO4, the solids were filtered off, the volatiles were evaporated in vacuum oven, and the residue was purified by column chromatography to obtain the desired product (26.8 mg, 70%) as a red-orange solid. Next, 5.5 g (16.9 mmol, 1 equiv.) N,N-bis(1 -oxido-2,2,6,6-tetramethylpiperidin-4-yl)amine was dissolved in 60 mL methanol, $NaHCO_3$ (7.12 g, 84.7 mmol) and CH_3I (5.28 mL, 84.5 mmol, 5 equiv.) was added subsequently. The mixture was sealed in a

250 mL thick-walled pressure bottle and the reaction was flux for 24 h. Upon completion, the solvent was removed by a rotary evaporator. The light-yellow solid was fully dissolved in 100 ml of water, the aqueous phase was washed with EtOAc (100 mL × 3). The aqueous phase was combined and evaporated. After drying, the powder was dissolved in 20.0 mL of deionized water and flushed through an anion exchange column with an Amberlite IRA-900 chloride form anion exchange resin. The solvent was removed, and the resulting orange solid is 6.6 g (yield: 90 %). The detailed synthetic method for all 21 i-TEMPODs as well as Bruker AVANCE 400 NMR spectrometer characterization is included in Supporting Information. Peaks in the NMR spectra correspond to the reduced TEMPO product as well as the phenylhydrazine reducing agent.

Electrochemical Characterization

A glassy carbon working electrode (CH Instruments, 0.0707 cm^2), a saturated calomel reference electrode (SCE, CH Instruments, +0.241 V vs. SHE), and a platinum wire counter electrode were used for both cyclic voltammetry (CV) and electrochemical impedance spectroscopy (EIS) measurements (PalmSens4 potentiostat instrument). The working electrode was polished with 1 μm, 0.3 μm, and 0.05 μm alumina slurry successively. All electrodes were rinsed with deionized water in between measurements. For each test, 15 mM i-TEMPOD in 1 M NaCl was used at room temperature (~22℃).

Theoretical Calculations

Full details can be found int Supplementral Information. In short, Ab Initio Molecular Dynamics (AIMD) simulations based on Density Functional Theory (DFT) using the Vienna Ab Initio Simulation Package (VASP) were performed. Calculations were performed using the projector augmented wave (PAW) method with Perdew-Burke-Ernzerhof pseudopotentials and the

generalized gradient approximation (GGA) exchange and correlation functional. Sampling of the Brillouin zone was performed with a single gamma-centered k-point. The planewave cutoff energy was set to 500 eV, and all calculations were performed with spin polarization enabled. For accurate treatment of van der Waals forces, the DFT-D3 method of Grimme was employed. AIMD calculations were performed in the constant mole number, volume and temperature (NVT) ensemble at a constant temperature of 500 ˚C, a timestep of 1 fs, and temperature was controlled using the Nose-Hoover thermostat.

Flow Cell Assembly and Testing

Commercial FXC Gen2 flow cell was used for RFB experiments. In brief, graphite plates (1/4-inch thickness, MWI) with serpentine flow channels were used as current collectors. Graphite felts (GFD 3 EA, SIGRACELL®) were pre-treated at 400 ℃ in air for 6 h before being used as electrodes on both sides of the cell. Selemion AMVN or DSVN (Asahi Glass Co., Ltd.,) was used as an anion-exchange membrane. The membrane was soaked in 1.0 M NaCl solution for more than 24 hours before use. A flow cell active area of 4 cm^2 was used for most RFB tests, other than N+TEMPOD RFBs with DSVN membrane, for which 16 cm^2 active area was used. The electrolytes were pumped through the flow channels by a peristaltic pump (Cole-Parmer Masterflex L/S). All RFB measurements were carried out in a N2 glove box (Vigor) with O^2 concentration below 1ppm. For long term cycling experiments with both previously reported TEMPO monomers and the newly designed i-TEMPODs, potentiostatic holds were not used at the end of cycles due to potential promotion of oxygen evolution reaction in the catholyte compartment, which would result in increased acidity with catholyte and anolyte degradation.

References

1. Sánchez-Díez, E. *et al.* Redox flow batteries: Status and perspective towards sustainable stationary energy storage. *J. Power Sources* **481**, 228804 (2021).
2. Wadia, C., Albertus, P. & Srinivasan, V. Resource constraints on the battery energy storage potential for grid and transportation applications. *J. Power Sources* **196**, 1593–1598 (2011).
3. Singh, V., Kim, S., Kang, J. & Byon, H. R. Aqueous organic redox flow batteries. *Nano Res.* **12**, 1988–2001 (2019).
4. Brushett, F. R., Aziz, M. J. & Rodby, K. E. On Lifetime and Cost of Redox-Active Organics for Aqueous Flow Batteries. *ACS Energy Lett.* **5**, 879–884 (2020).
5. Gentil, S., Reynard, D. & Girault, H. H. Aqueous organic and redox-mediated redox flow batteries: a review. *Curr. Opin. Electrochem.* **21**, 7–13 (2020).
6. Luo, J., Hu, B., Hu, M., Zhao, Y. & Liu, T. L. Status and Prospects of Organic Redox Flow Batteries toward Sustainable Energy Storage. *ACS Energy Letters* vol. 4 2220–2240 (2019).
7. Winsberg, J., Hagemann, T., Janoschka, T., Hager, M. D. & Schubert, U. S. Redox-Flow Batteries: From Metals to Organic Redox-Active Materials. *Angew. Chemie - Int. Ed.* **56**, 686–711 (2017).
8. Ding, Y., Zhang, C., Zhang, L., Zhou, Y. & Yu, G. Molecular engineering of organic electroactive materials for redox flow batteries. *Chemical Society Reviews* vol. 47 69–103 (2018).
9. Liu, Y. *et al.* Organic electrolytes for aqueous organic flow batteries. *Mater. Today Energy* **20**, (2021).
10. Cao, J., Tian, J., Xu, J. & Wang, Y. Organic Flow Batteries: Recent Progress and Perspectives. *Energy and Fuels* **34**, 13384–13411 (2020).
11. Luo, J., Wang, A. P., Hu, M. & Liu, T. L. Materials challenges of aqueous redox flow batteries. *MRS Energy Sustain.* **9**, 1–12 (2022).
12. Kwabi, D. G., Ji, Y. & Aziz, M. J. Electrolyte Lifetime in Aqueous Organic Redox Flow Batteries: A Critical Review. *Chem. Rev.* **120**, 6467–6489 (2020).
13. Zhong, F., Yang, M., Ding, M. & Jia, C. Organic Electroactive Molecule-Based Electrolytes for Redox Flow Batteries: Status and Challenges of Molecular Design. *Frontiers in Chemistry* vol. 8 451 (2020).
14. Wu, M. *et al.* Extremely Stable Anthraquinone Negolytes Synthesized from Common Precursors. *Chem* **6**, 1432–1442 (2020).
15. Ji, Y. *et al.* A Phosphonate-Functionalized Quinone Redox Flow Battery at Near-Neutral pH with Record Capacity Retention Rate. *Adv. Energy Mater.* **9**, 1900039 (2019).
16. Kwabi, D. G. *et al.* Alkaline Quinone Flow Battery with Long Lifetime at pH 12. *Joule* **2**, 1894–1906 (2018).
17. Yang, Z. *et al.* Alkaline Benzoquinone Aqueous Flow Battery for Large-Scale Storage of Electrical Energy. *Adv. Energy Mater.* **8**, 1702056 (2018).
18. Gerhardt, M. R. *et al.* Anthraquinone Derivatives in Aqueous Flow Batteries. *Adv. Energy Mater.* **7**, 1601488 (2017).
19. Lin, K. *et al.* Alkaline quinone flow battery. *Science (80-.).* **349**, 1529–1532 (2015).
20. Wu, M., Bahari, M., Fell, E. M., Gordon, R. G. & Aziz, M. J. High-performance anthraquinone with potentially low cost for aqueous redox flow batteries. *J. Mater. Chem. A* **9**, 26709–26716 (2021).
21. Jing, Y. *et al.* Anthraquinone Flow Battery Reactants with Nonhydrolyzable Water-Solubilizing Chains Introduced via a Generic Cross-Coupling Method. *ACS Energy Lett.* **7**,

226–235 (2022).
22. Wu, M. *et al.* Highly Stable, Low Redox Potential Quinone for Aqueous Flow Batteries. *Batter. Supercaps* e202200009 (2022) doi:10.1002/batt.202200009.
23. Symons, P. Quinones for redox flow batteries. *Curr. Opin. Electrochem.* **29**, (2021).
24. Jin, S. *et al.* A Water-Miscible Quinone Flow Battery with High Volumetric Capacity and Energy Density. *ACS Energy Lett.* **4**, 1342–1348 (2019).
25. Beh, E. S. *et al.* A neutral pH aqueous organic- organometallic redox flow battery with extremely high capacity retention. *ACS Energy Lett.* **2**, 639–644 (2017).
26. Jang, S.-S. *et al.* Methyl Viologen Anolyte Introducing Nitrate as Counter-Anion for an Aqueous Redox Flow Battery. *J. Electrochem. Soc.* **168**, 100532 (2021).
27. Luo, J., Hu, B., Debruler, C. & Liu, T. L. A π-Conjugation Extended Viologen as a Two-Electron Storage Anolyte for Total Organic Aqueous Redox Flow Batteries. *Angew. Chemie - Int. Ed.* **57**, 231–235 (2018).
28. Debruler, C., Hu, B., Moss, J., Luo, J. & Liu, T. L. A Sulfonate-Functionalized Viologen Enabling Neutral Cation Exchange, Aqueous Organic Redox Flow Batteries toward Renewable Energy Storage. *ACS Energy Lett.* **3**, 663–668 (2018).
29. DeBruler, C. *et al.* Designer Two-Electron Storage Viologen Anolyte Materials for Neutral Aqueous Organic Redox Flow Batteries. *Chem* **3**, 961–978 (2017).
30. Jin, S. *et al.* Near Neutral pH Redox Flow Battery with Low Permeability and Long-Lifetime Phosphonated Viologen Active Species. *Adv. Energy Mater.* **10**, 2000100 (2020).
31. Liu, Y. *et al.* Screening Viologen Derivatives for Neutral Aqueous Organic Redox Flow Batteries. *ChemSusChem* **13**, 2245–2249 (2020).
32. Liu, T., Wei, X., Nie, Z., Sprenkle, V. & Wang, W. A Total Organic Aqueous Redox Flow Battery Employing a Low Cost and Sustainable Methyl Viologen Anolyte and 4-HO-TEMPO Catholyte. *Adv. Energy Mater.* **6**, 1501449 (2016).
33. Hu, B. *et al.* Improved radical stability of viologen anolytes in aqueous organic redox flow batteries. *Chem. Commun.* **54**, 6871–6874 (2018).
34. Liu, L., Yao, Y., Wang, Z. & Lu, Y. C. Viologen radical stabilization by molecular spectators for aqueous organic redox flow batteries. *Nano Energy* **84**, 105897 (2021).
35. Pang, S., Wang, X., Wang, P. & Ji, Y. Biomimetic Amino Acid Functionalized Phenazine Flow Batteries with Long Lifetime at Near-Neutral pH. *Angew. Chemie - Int. Ed.* **60**, 5289–5298 (2021).
36. Hollas, A. *et al.* A biomimetic high-capacity phenazine-based anolyte for aqueous organic redox flow batteries. *Nat. Energy* **3**, 508–514 (2018).
37. Xu, J., Pang, S., Wang, X., Wang, P. & Ji, Y. Ultrastable aqueous phenazine flow batteries with high capacity operated at elevated temperatures. *Joule* **5**, 2437–2449 (2021).
38. Romadina, E. I., Komarov, D. S., Stevenson, K. J. & Troshin, P. A. New phenazine based anolyte material for high voltage organic redox flow batteries. *Chem. Commun.* **57**, 2986–2989 (2021).
39. Wang, C. *et al.* Molecular Design of Fused-Ring Phenazine Derivatives for Long-Cycling Alkaline Redox Flow Batteries. **45**, 41 (2020).
40. De La Cruz, C. *et al.* New insights into phenazine-based organic redox flow batteries by using high-throughput DFT modelling. *Sustain. Energy Fuels* **4**, 5513–5521 (2020).
41. Janoschka, T., Martin, N., Hager, M. D. & Schubert, U. S. An Aqueous Redox-Flow Battery with High Capacity and Power: The TEMPTMA/MV System. *Angew. Chemie - Int. Ed.* **55**, 14427–14430 (2016).

42. Nolte, O., Rohland, P., Ueberschaar, N., Hager, M. D. & Schubert, U. S. Stability of TMA-TEMPO-based aqueous electrolytes for redox-flow batteries. *J. Power Sources* **525**, 230996 (2022).
43. Liu, B., Tang, C. W., Jiang, H., Jia, G. & Zhao, T. Carboxyl-functionalized Tempo catholyte enabling high-cycling-stability and high-energy-density aqueous organic redox flow batteries. *ACS Sustain. Chem. Eng.* **9**, 6258–6265 (2021).
44. Schubert, U. S. *et al.* Structural alterations on the TEMPO scaffold and their impact on the performance as active materials for redox flow batteries. *Mater. Adv.* (2022) doi:10.1039/d1ma00663k.
45. Pan, M. *et al.* Reversible Redox Chemistry in Pyrrolidinium-Based TEMPO Radical and Extended Viologen for High-Voltage and Long-Life Aqueous Redox Flow Batteries. *Adv. Energy Mater.* **12**, 2103478 (2022).
46. Hu, B., Hu, M., Luo, J. & Liu, T. L. A Stable, Low Permeable TEMPO Catholyte for Aqueous Total Organic Redox Flow Batteries. *Adv. Energy Mater.* **12**, 1–5 (2022).
47. Liu, Y. *et al.* A Long-Lifetime All-Organic Aqueous Flow Battery Utilizing TMAP-TEMPO Radical. *Chem* **5**, 1861–1870 (2019).
48. Zhou, W. *et al.* Fundamental properties of TEMPO-based catholytes for aqueous redox flow batteries: effects of substituent groups and electrolytes on electrochemical properties, solubilities and battery performance. *RSC Adv.* **10**, 21839–21844 (2020).
49. Ohira, A., Funaki, T., Ishida, E., Kim, J. D. & Sato, Y. Redox-Flow Battery Operating in Neutral and Acidic Environments with Multielectron-Transfer-Type Viologen Molecular Assembly. *ACS Appl. Energy Mater.* **3**, 4377–4383 (2020).
50. Silva, W., Zanatta, M., Ferreira, A. S., Corvo, M. C. & Cabrita, E. J. Revisiting ionic liquid structure‐property relationship: A critical analysis. *Int. J. Mol. Sci.* **21**, 1–37 (2020).
51. Hayes, R., Warr, G. G. & Atkin, R. Structure and Nanostructure in Ionic Liquids. *Chem. Rev.* **115**, 6357–6426 (2015).
52. Suo, L. *et al.* "Water-in-Salt" Electrolyte Makes Aqueous Sodium-Ion Battery Safe, Green, and Long-Lasting. *Adv. Energy Mater.* **7**, (2017).
53. Suo, L. *et al.* 'water-in-Salt' electrolytes enable green and safe Li-ion batteries for large scale electric energy storage applications. *J. Mater. Chem. A* **4**, 6639–6644 (2016).
54. Suo, L. *et al.* 'Water-in-salt' electrolyte enables high-voltage aqueous lithium-ion chemistries. *Science (80-.).* **350**, 938–943 (2015).
55. Jaumaux, P. *et al.* Localized Water-In-Salt Electrolyte for Aqueous Lithium-Ion Batteries. *Angew. Chemie - Int. Ed.* **60**, 19965–19973 (2021).
56. McEldrew, M., Goodwin, Z. A. H., Kornyshev, A. A. & Bazant, M. Z. Theory of the Double Layer in Water-in-Salt Electrolytes. *J. Phys. Chem. Lett.* **9**, 5840–5846 (2018).
57. Martins, V. L. & Torresi, R. M. Water-in-salt electrolytes for high voltage aqueous electrochemical energy storage devices. *Curr. Opin. Electrochem.* **21**, 62–68 (2020).
58. Kühnel, R.-S., Reber, D. & Battaglia, C. Perspective—Electrochemical Stability of Water-in-Salt Electrolytes. *J. Electrochem. Soc.* **167**, 070544 (2020).
59. Perry, M. L., Rodby, K. E. & Brushett, F. R. Untapped Potential: The Need and Opportunity for High-Voltage Aqueous Redox Flow Batteries. *ACS Energy Lett.* **7**, 659–667 (2022).
60. Lv, X.-L. *et al.* The Economically Sustainable Hydrothermal Synthesis of Dextrosil-Viologen as a Robust Anolyte in Aqueous Redox Flow Batteries. (2022) doi:10.26434/CHEMRXIV-2022-KZZN4.
61. Debruler, C., Hu, B., Moss, J., Luo, J. & Liu, T. L. A Sulfonate-Functionalized Viologen

Enabling Neutral Cation Exchange, Aqueous Organic Redox Flow Batteries toward Renewable Energy Storage. *ACS Energy Lett.* **3**, 663–668 (2018).
62. Feng, R. *et al.* Reversible ketone hydrogenation and dehydrogenation for aqueous organic redox flow batteries. *Science (80-.).* **372**, 836–840 (2021).
63. Luo, J. *et al.* Unprecedented Capacity and Stability of Ammonium Ferrocyanide Catholyte in pH Neutral Aqueous Redox Flow Batteries. *Joule* **3**, 149–163 (2019).
64. Li, X. *et al.* Symmetry-breaking design of an organic iron complex catholyte for a long cyclability aqueous organic redox flow battery. *Nat. Energy* 1–9 (2021) doi:10.1038/s41560-021-00879-6.
65. Chen, Q. *et al.* Designer Ferrocene Catholyte for Aqueous Organic Flow Batteries. *ChemSusChem* **14**, 1295–1301 (2021).
66. DeBruler, C. *et al.* Designer Two-Electron Storage Viologen Anolyte Materials for Neutral Aqueous Organic Redox Flow Batteries. *Chem* **3**, 961–978 (2017).
67. Hu, B., Debruler, C., Rhodes, Z. & Liu, T. L. Long-Cycling aqueous organic Redox flow battery (AORFB) toward sustainable and safe energy storage. *J. Am. Chem. Soc.* **139**, 1207–1214 (2017).
68. Beh, E. S. *et al.* A Neutral pH Aqueous Organic–Organometallic Redox Flow Battery with Extremely High Capacity Retention. *ACS Energy Lett.* **2**, 639–644 (2017).

Acknowledgments

D.F. acknowledges the start-up funds from the University of Wisconsin-Madison, WARF Accelerator Project (AP) via 197500-135-AAJ4936, and Draper Technology Innovation Fund (TIF) under 197500-135-AAJ4236. P.S. thanks the support by Vice Chancellor for Research and Graduate Education (VCRGE) via 1975XX-135-AAI2755. S.J., W.L., and H.C.F. thank the support by the King Abdullah University of Science and Technology (KAUST) Office of Sponsored Research (OSR) under award no. OSR-2017-CRG6-3453.02. C.J.C. thanks the support from the Ministry of Science and Technology (MOST) in Taiwan via 109-2917-I-564-010. The authors would like to thank I. Guzei for assistance with data collection of single crystal X-ray diffraction. The Bruker Quazar APEX2 was purchased by UW–Madison Department of Chemistry with a portion of a generous gift from Paul J. and Margaret M. Bender. The Bruker AVANCE 400 NMR spectrometer was supported by NSF grant CHE-1048642.

Conflict of Interest

Wisconsin Alumni Research Foundation (WARF) has filed a patent application on the materials described in this paper.